J Therm Spray Tech (2022) 31:1366–1374
https://doi.org/10.1007/s11666-021-01297-6

PEER REVIEWED

Influence of Aluminum and Molybdenum on the Microstructure and Corrosion Behavior of Thermally Sprayed High-Entropy Alloy Coatings

Martin Löbel[1] · Thomas Lindner[1] · Maximilian Grimm[1] · Lisa-Marie Rymer[1] · Thomas Lampke[1]

Submitted: 8 September 2021 / in revised form: 28 November 2021 / Accepted: 29 November 2021 / Published online: 28 December 2021

Abstract High-entropy alloys (HEAs) have shown a wide range of promising structural and functional properties. By the application of coating technology, an economical exploitation can be achieved. The high wear and corrosion resistance of HEAs make them particularly interesting for the application as protective coatings. Especially for alloys with a high chromium content, a high corrosion resistance has been revealed. For the current investigations, the equimolar HEA CrFeCoNi with a single-phase face centered cubic structure is considered as a base alloy system. To increase the corrosion resistance as well as the hardness and strength, the influence of the alloying elements aluminum and molybdenum is analyzed. For the current investigations, the high kinetic process high-velocity oxygen fuel thermal spraying (HVOF) has been considered to produce coatings with a low porosity and oxide content. Feedstock is produced by inert gas atomization. The influence of the alloy composition on the microstructure, phase formation and resulting property profile is studied in detail. A detailed analysis of the corrosion resistance and underlying mechanisms is conducted. The pitting and passivation behavior are investigated by potentiodynamic polarization measurements in NaCl and H_2SO_4 electrolyte. A distinct improvement of the corrosion resistance can be achieved for the alloy $Al_{0.3}CrFeCoNiMo_{0.2}$.

Keywords coating · corrosion · HEA · high-entropy alloy · HVOF · microstructure

Introduction

The multiprincipal alloying approach of high-entropy alloys (HEAs) has gained intensive research interest in the past almost two decades. Despite the lack of one principal alloying element, the formation of solid solutions with face centered cubic (fcc) or body centered cubic (bcc) structure could be achieved, whereas complex phases were suppressed. One of the first alloys, where the formation of a single-phase fcc structure was reported, is the quinary alloy CrMnFeCoNi (Ref 1). Subsequent studies also proved the formation of a single-phase fcc structure for the quaternary alloy CrFeCoNi (Ref 2). A high ductility was typically observed for HEAs with an fcc structure. However, their strength and hardness are reduced in comparison with HEAs with a bcc structure (Ref 3). The alloy CrFeCoNi served as a base alloy for many previous studies, where the influence of additional alloying elements was investigated. A strong influence of the aluminum content on the phase composition and resulting properties was proven. Whereas the fcc structure is retained for low contents, a further increase causes the stabilization of a bcc structure. Due to the high atomic radius and hence lattice distortion, an increase in hardness can already be achieved for low

This article is part of a special topical focus in the Journal of Thermal Spray Technology on High Entropy Alloy and Bulk Metallic Glass Coatings. The issue was organized by Dr. Andrew S.M. Ang, Swinburne University of Technology; Prof. B.S. Murty, Indian Institute of Technology Hyderabad; Distinguished Prof. Jien-Wei Yeh, National Tsing Hua University; Prof. Paul Munroe, University of New South Wales; Distinguished Prof. Christopher C. Berndt, Swinburne University of Technology. The issue organizers were mentored by Emeritus Prof. S. Ranganathan, Indian Institute of Sciences.

✉ Martin Löbel
martin.loebel.ww@gmail.com

[1] Materials and Surface Engineering Group, Institute of Materials Science and Engineering, Chemnitz University of Technology, 09107 Chemnitz, Germany

aluminum contents where the fcc structure is retained. Due to the stabilization of a bcc structure, the highest hardness values have been measured for higher aluminum contents (Ref 4, 5).

Besides the chemical composition, the production conditions have shown a distinct influence on the phase formation and properties. High cooling rates resulted in the suppression of additional phases for the equimolar alloy AlCrFeCoNi (Ref 6, 7).

The fcc alloy $Al_{0.3}$CrFeCoNi also served as a starting point to investigate the influence of additional alloying elements. Shun et al. investigated the influence of molybdenum and titanium additions. For the as-cast state, a single-phase fcc structure was formed in each case, whereas an increase in hardness was achieved by the addition of molybdenum and titanium due to solid solution strengthening. Age-hardening and the formation of precipitates resulted in a further increase (Ref 8). Investigations by Zhuang et al. also proved the increase in hardness and strength by the addition of molybdenum in the alloy system AlCrFeCoNiMo. However, the ductility was reduced for high molybdenum contents due to the formation of the (Cr, Mo)-rich and brittle σ-phase (Ref 9).

Early studies of HEAs focused especially on structural properties. However, also interesting functional properties, e.g., wear and corrosion resistance, were revealed (Ref 10, 11). For the alloy system AlCrFeCoNi, a high corrosion resistance was proven for measurements in NaCl and H_2SO_4 electrolytes (Ref 12, 13). In comparison with the stainless steel AISI 304, an enhanced corrosion resistance in NaCl electrolyte could be achieved for the HEA $Al_{0.1}$CrFeCoNi (Ref 14). The alloying element molybdenum, which is also very important for improving the corrosion and pitting resistance of stainless steels, has been investigated to optimize the properties of HEAs (Ref 15). Chou et al. showed that the pitting resistance in aqueous NaCl electrolyte can be improved by the addition of molybdenum for the alloy system TiCrFeCoNiMo (Ref 16). Furthermore, Wang et al. investigated the passivation behavior in H_2SO_4 electrolyte for the alloy system CrFeCoNiMo. The addition of molybdenum caused an extensive passive region and a reduction of the corrosion current density (Ref 17). However, a detrimental effect was observed for the alloy system CrFeCoNiMo investigated in NaCl and H_2SO_4 electrolytes for high molybdenum contents due to an increased content of the σ-phase (Ref 18). In accordance with many conventional alloys, the formation of passive films especially for Cr and Mo containing alloys is crucial for the corrosion resistance of HEAs (Ref 12, 15, 19).

Whereas the focus of most studies has been on cast bulk alloys, HEAs are also promising candidates for the application as protective coatings due to their high wear and corrosion resistance (Ref 20). Thermal spray processes offer great flexibility and enable the coating of various substrates. These processes have already been widely studied regarding their suitability to process HEAs (Ref 21). Especially high kinetic processes like high-velocity oxygen fuel (HVOF) thermal spraying are suitable for the deposition of coatings with a low content of structural defects (e. g. pores and oxides) (Ref 20-22).

In the present study, the influence of the alloying elements aluminum and molybdenum on the corrosion behavior of the single-phase HEA CrFeCoNi with fcc structure is investigated. Protective coatings are deposited by HVOF thermal spraying the HEAs CrFeCoNi, $Al_{0.3}$CrFeCoNi and $Al_{0.3}$CrFeCoNi$Mo_{0.2}$. The microstructure, phase formation and corrosion behavior are studied in detail. For the investigation of the pitting and passivation behavior, potentiodynamic measurements are conducted in NaCl and H_2SO_4 electrolyte.

Materials and Methods

Feedstock powders of the HEAs CrFeCoNi, $Al_{0.3}$CrFeCoNi ($Al_{0.3}$) and $Al_{0.3}$CrFeCoNi$Mo_{0.2}$ ($Al_{0.3}Mo_{0.2}$) were produced by the company NANOVAL GmbH & Co. KG (Berlin, Germany) using an inert gas atomization process. For the processing by thermal spraying, the powders were classified to a fraction of − 50 +20 µm (− d90 +d10) by air classification. The particle size distribution was measured by laser diffraction analyses using a Cilas 920 device (Cilas, Orléans, France). The phase composition was determined by x-ray diffraction (XRD) using a D8 Discover diffractometer (Bruker AXS, Billerica, MA, USA) equipped with a 1D Lynxeye XE detector (Bruker AXS, Billerica, MA, USA). All measurements have been conducted using monochromatic Co Kα radiation in a diffraction range (2θ) of 20° to 130°. For the analyses of the microstructure, cross-sections have been prepared by standard metallographic procedures and investigated in the scanning electron microscope (SEM) LEO 1455VP (Zeiss, Jena, Germany). Material contrast was visualized by applying a backscattered electron detector (BSD). Furthermore, the chemical composition was determined with the coupled energy dispersive x-ray spectroscopy (EDS) detector. All measurements have been conducted with an acceleration voltage of 25 kV.

Coating deposition was conducted with the liquid fueled HVOF thermal spray system K2 (GTV Verschleißschutz GmbH, Luckenbach, Germany) using the powder feeding system PFW 4/3 S (GTV Verschleißschutz GmbH, Luckenbach, Germany). For all investigations, two powder feeders were applied. Prior to the coating process, the stainless-steel substrates (EN 1.4404) with a diameter of

40 mm and a thickness of 6 mm were prepared by corundum blasting. A pressure of 2.5 bar and the blasting medium Alodur EK F 24 have been used. Previous investigations revealed roughness values of R_a: 5,4 µm and R_z: 37,8 µm for this routine. The coating parameters are summarized in Table 1.

The microstructure, phase composition and chemical composition have been analyzed in accordance with the routine described for the powder classification. The microhardness HV 0.3 has been determined in cross-sections using a Wilson Tukon 1102 device (Buehler, Uzwil, Switzerland). The mean value and standard deviation have been derived from ten single measurements.

The focus of the current investigations was on the corrosion behavior. Therefore, samples have been prepared by grinding the surface down to Grit 4000 (US#1200). Potentiodynamic polarization measurements have been conducted to determine the resistance against pitting and the passivation behavior. An IM6 potentiostat (ZAHNER-elektrik GmbH & Co. KG, Kronach, Germany) has been applied for all measurements to investigate a circular area with a diameter of 10 mm. All tests have been conducted at room temperature with a three-electrode arrangement. A Pt sheet (20×20 mm^2) has been used as a counter electrode, whereas an Ag/AgCl (saturated KCl) electrode served as a reference electrode. Prior to every measurement, the open circuit potential (OCP) has been measured for 15 min. The pitting resistance was investigated using 0.5 M NaCl electrolyte and a scan rate of 0.1 mV/s for a polarization range of − 150 to + 700 mV in relation to the OCP. Furthermore, the passivation behavior has been investigated by measurements in 0.05 M H_2SO_4 electrolyte and a scan rate of 0.5 mV/s for an expanded polarization range from − 150 to + 1800 mV in relation to the OCP. Due to the formation of a distinct passivity area, the measurement within a large potential range is necessary to determine the breakthrough potential.

The potentiodynamic polarization curves were evaluated by fitting the Butler–Volmer equation to determine the corrosion potential (E_{corr}) and the corrosion current density (i_{corr}) (Ref 23, 24). At least three single measurements have been considered to determine the average value and standard deviation.

For the investigation of the corrosion behavior, additional measurements have been conducted and interrupted at a defined current density of 2 mA/cm^2. The surface of the samples was investigated by SEM.

Results and Discussion

Feedstock Characterization

Prior to the coating deposition, a detailed characterization of the feedstock powder has been conducted. Cross-sections of the powders, investigated in SEM, are shown in Fig. 1.

Predominantly spherical particles can be observed for all investigated feedstock powders due to the production by gas atomization. Only minor accumulations of satellites at bigger particles occur. Within single particles, no material contrast can be observed for CrFeCoNi. Also, for the aluminum- and molybdenum-containing alloys no material contrast occurs, indicating the formation of a single-phase state for the investigated production conditions. The particle size distribution has been investigated by laser diffraction analyses to determine the characteristic values d10, d50 and d90. A summary of the results is presented in Table 2.

The determined particle size distribution of all investigated powders is in good accordance with the specifications (− 50 +20 µm). Only for the CrFeCoNi powder the characteristic values d90 and d10 are slightly shifted to higher values.

The phase composition was investigated by means of XRD. The resulting diffractograms are shown in Fig. 2.

For the CrFeCoNi powder, solely diffractions peaks of a chemically disordered fcc phase with A1 structure occur, which is in accordance with previous investigations on cast alloys (Ref 2). In accordance with the microstructural investigations, a single-phase state can be confirmed for the $Al_{0.3}$ and $Al_{0.3}Mo_{0.2}$ feedstock. Previously published results have proven additional phases for these alloys in dependence of the heat treatment state (Ref 8). Due to the high cooling rates in the atomization process, additional phases are suppressed. In comparison with the base alloy system CrFeCoNi the addition of aluminum and molybdenum causes a shift of the diffraction peaks toward lower diffraction angles, indicating an increased lattice parameter.

Table 1 HVOF coating parameters for the deposition of CrFeCoNi, $Al_{0.3}$ and $Al_{0.3}Mo_{0.2}$.

O_2, l/min	Kerosene, l/h	λ	Carrier gas (Ar) flow, l/min	nozzle	Powder feed rate, g/min	Spraying distance, mm	Surface speed, m/min	Spray-path offset, mm	Coating layers
850	22.5	1.1	2 × 11	100/12	2 × 35	360	60	5	11

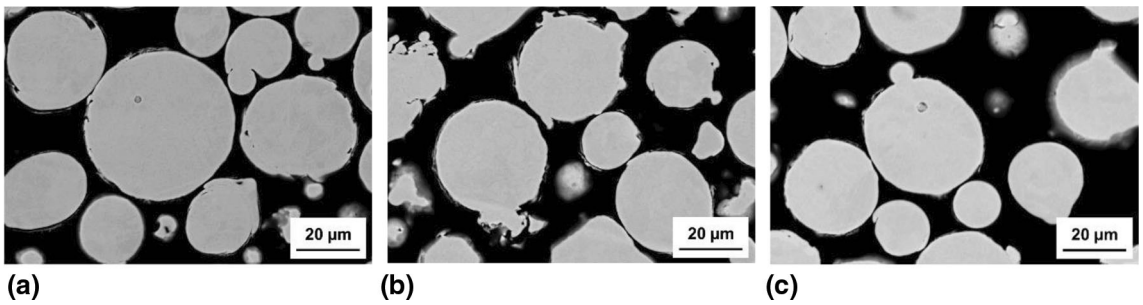

Fig. 1 Cross-sections of atomized powders: (a) CrFeCoNi, (b) $Al_{0.3}$ and (c) $Al_{0.3}Mo_{0.2}$ investigated in SEM (BSD)

Table 2 Particle size distribution of inert gas atomized CrFeCoNi, $Al_{0.3}$ and $Al_{0.3}Mo_{0.2}$ HEA powder in µm.

	d10	d50	d90
CrFeCoNi	22.8	36.1	55.4
$Al_{0.3}$	20.9	32.9	50.1
$Al_{0.3}Mo_{0.2}$	20.9	33.4	50.6

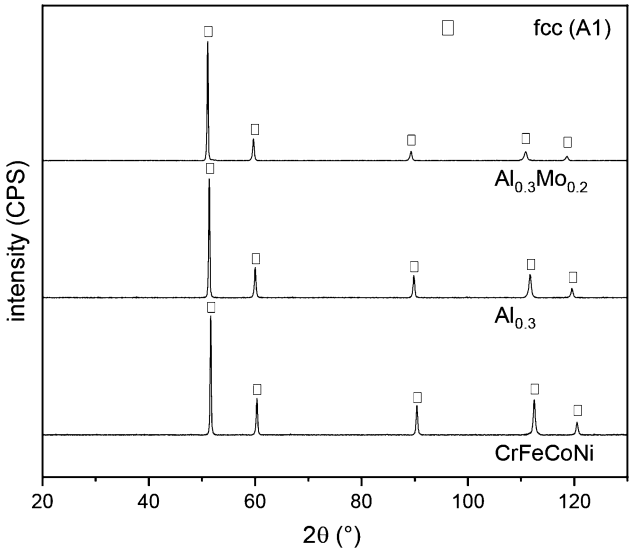

Fig. 2 Diffractograms of CrFeCoNi, $Al_{0.3}$ and $Al_{0.3}Mo_{0.2}$ feedstock powder

Coating Characterization

For the investigation of the coating microstructure, cross-sections were prepared and investigated by SEM (Fig. 3).

A lamellar coating structure comprised of single spray particles is observed for all three coatings types. Only minor structural defects (pores, oxides) are present due to the usage of gas-atomized powder (Ref 25) and the application of the high-kinetic process HVOF thermal spraying. Also, at higher magnification no distinct material contrast is observed within single-spray particles, indicating that the single-phase state of the feedstock powder is retained for the coatings. The chemical composition of the coatings was investigated by EDS. Furthermore, the chemical composition of the feedstock powder was determined to detect possible deviations caused by the coating process. The measured values and the nominal compositions are summarized in Table 3.

The measured values of the feedstock powder and HVOF coating for the HEA CrFeCoNi are in good accordance with the nominal values. Deviations below 1 at.% occur, which are in the range of the accuracy of the method. For the $Al_{0.3}$ and $Al_{0.3}Mo_{0.2}$ feedstock powder, the deviation of the aluminum content exceeds 1 at.% in comparison with the nominal composition. All investigated coatings only reveal minor differences of the chemical composition in comparison with the feedstock powder, showing that no distinct changes are induced by the coating process.

The phase composition of the HEA coatings was investigated by means of XRD. In Fig. 4, the diffractograms are summarized.

In accordance with the feedstock powder, solely diffraction peaks of an fcc phase with A1 structure occur for the CrFeCoNi coating, showing that the single-phase state is retained. Also, for the $Al_{0.3}$ and $Al_{0.3}Mo_{0.2}$ HVOF coatings no additional diffraction peaks occur in comparison to the feedstock powder. Due to the low thermal energy input of the coating process, the single-phase state is retained. In comparison with the base alloy CrFeCoNi, the diffraction peaks of $Al_{0.3}$ and $Al_{0.3}Mo_{0.2}$ are shifted toward lower values, indicating a change of the lattice parameter. The lattice parameters derived from the XRD measurements are summarized in Table 4. A lattice parameter of 3.57 Å was determined for the CrFeCoNi powder and HVOF coatings. Alloying with aluminum causes a slight increase in the lattice parameter due to the increased atomic size differences and hence increased lattice distortion (Ref 4). The highest lattice parameter of 3.60 Å was measured for the alloy $Al_{0.3}Mo_{0.2}$. For all investigated alloys, no distinct influence of the coating process on the lattice parameter can be observed.

The influence of the alloying elements aluminum and molybdenum on the resulting properties was investigated

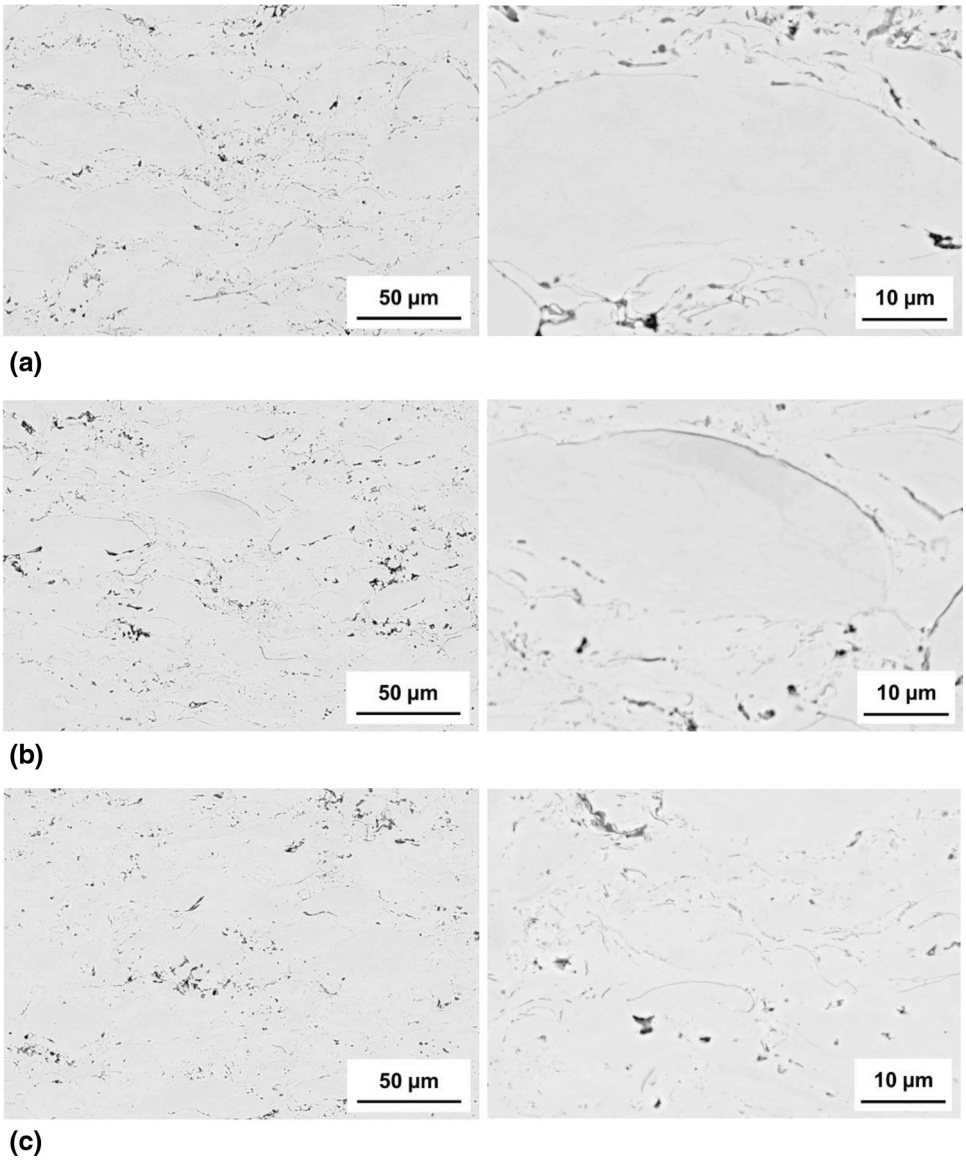

Fig. 3 Microstructure of HVOF coatings: (a) CrFeCoNi, (b) $Al_{0.3}$ and (c) $Al_{0.3}Mo_{0.2}$ investigated in SEM (BSD)

Table 3 Nominal and measured (EDS) chemical composition of the feedstock powder and HVOF coatings, in at.%.

Alloy		Al	Cr	Fe	Co	Ni	Mo
CrFeCoNi	Nominal	*0.0*	*25.0*	*25.0*	*25.0*	*25.0*	*0.0*
CrFeCoNi	Powder	0.0	25.1	25.3	24.6	25.3	0.0
CrFeCoNi	HVOF	0.0	25.2	25.0	24.8	25.1	0.0
$Al_{0.3}$	Nominal	*7.0*	*23.3*	*23.3*	*23.3*	*23.3*	*0.0*
$Al_{0.3}$	Powder	8.8	23.1	22.9	22.5	22.7	0.0
$Al_{0.3}$	HVOF	8.9	22.9	23.1	22.3	22.7	0.0
$Al_{0.3}Mo_{0.2}$	Nominal	*6.7*	*22.2*	*22.2*	*22.2*	*22.2*	*4.4*
$Al_{0.3}Mo_{0.2}$	Powder	8.0	21.8	22.3	21.3	21.4	5.2
$Al_{0.3}Mo_{0.2}$	HVOF	7.8	21.7	22.4	21.2	21.5	5.4

by microhardness measurements in a first step. The results are summarized in Fig. 5.

The lowest microhardness of 350 ± 20 HV 0.3 was measured for the CrFeCoNi coating. Alloying with aluminum causes an increase to a value of 390 ± 30 HV 0.3 due to the increased atomic size differences and lattice distortion. The highest hardness value of 400 ± 20 HV 0.3 was determined for the alloy $Al_{0.3}Mo_{0.2}$.

Corrosion Behavior

The pitting and passivation behavior of the HEA coatings were investigated by potentiodynamic polarization measurements in NaCl and H_2SO_4 electrolytes. Exemplary potentiodynamic polarization curves are shown in Fig. 6.

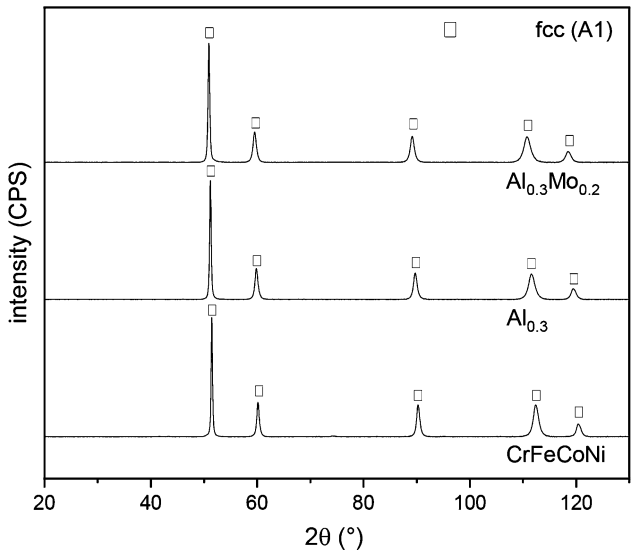

Fig. 4 Diffractograms of CrFeCoNi, $Al_{0.3}$ and $Al_{0.3}Mo_{0.2}$ HVOF coatings

Table 4 Lattice parameter of the fcc (A1) phase determined by XRD for the CrFeCoNi, $Al_{0.3}$ and $Al_{0.3}Mo_{0.2}$ feedstock powder and HVOF coatings.

Alloy	State	Lattice parameter, Å
CrFeCoNi	Powder	3.57
CrFeCoNi	HVOF	3.57
$Al_{0.3}$	Powder	3.58
$Al_{0.3}$	HVOF	3.59
$Al_{0.3}Mo_{0.2}$	Powder	3.60
$Al_{0.3}Mo_{0.2}$	HVOF	3.60

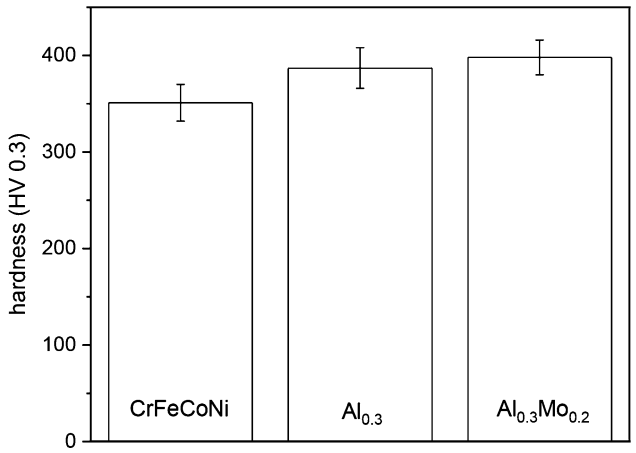

Fig. 5 Microhardness (HV 0.3) of CrFeCoNi, $Al_{0.3}$ and $Al_{0.3}Mo_{0.2}$ HVOF coatings.

The investigations in NaCl electrolyte reveal a distinct influence of the chemical composition on the corrosion behavior. For the CrFeCoNi coatings, the curve shows discontinuities. Furthermore, pronounced deviations between single measurements occur. Therefore, no reliable evaluation of E_{corr} and i_{corr} was possible. The curves of the $Al_{0.3}$ and $Al_{0.3}Mo_{0.2}$ are shifted toward higher potentials, indicating a more noble behavior, especially caused by the element molybdenum (Ref 26). In comparison with the base alloy CrFeCoNi, the current density is reduced in the complete potential range (relative to the E_{corr}). While the corrosion current densities i_{corr} of the alloys $Al_{0.3}$ and $Al_{0.3}Mo_{0.2}$ differ only slightly, there are considerable differences in the anodic behavior of the polarization curves. Whereas $Al_{0.3}$ shows an active behavior similar to the initial alloy, the measurements of alloy $Al_{0.3}Mo_{0.2}$ indicate a considerably more passive behavior, which is noticeable in a low current density up to high polarization ranges, indicating reduced corrosion reactions and a higher resistance against pitting. The formation of a passivation region in NaCl is attributed to the presence of molybdenum (Ref 17, 18, 26).

The investigation of the passivation behavior in H_2SO_4 electrolyte reveals a distinct passive region for all considered HEA coatings. This finding indicates that a dense passive film has probably formed on all surfaces examined. Further detailed investigations are required to elucidate the presence of such a passive film and its composition. In particular, the element molybdenum dissolved in the solid solution is known to enhance the protective effect of the formed passive film (Ref 17, 19, 26, 27). All the investigated coatings show significantly higher corrosion current densities in the H_2SO_4 electrolyte than in the NaCl electrolyte. This was also observed for $CrFeCoNiMo_{\chi}$ (Ref 17, 18, 26). For the measurements in H_2SO_4, alloying with aluminum does not cause a significant change of the potentiodynamic polarization curve in comparison with the alloy CrFeCoNi. However, a significant influence of the alloying element molybdenum can be observed for the $Al_{0.3}Mo_{0.2}$ coating. The E_{corr} is shifted toward higher values. Furthermore, the current density is distinctly reduced. In the passive region, the current density is similar to the CrFeCoNi and $Al_{0.3}$ coatings. The breakthrough potential, which marks the end of the passive region, is similar for all three investigated coating types. The potentiodynamic polarization curves have been evaluated to determine the characteristic values E_{corr} and i_{corr}, Table 5.

The investigation of the passivation behavior in H_2SO_4 electrolyte revealed a distinct influence of the alloy composition. Alloying with aluminum does not cause a significant change of the E_{corr}, whereas a significant increase and hence more noble behavior were observed for the molybdenum-containing coating $Al_{0.3}Mo_{0.2}$. The investigation of i_{corr} reveals a similar behavior. Alloying with aluminum does not cause an alteration of i_{corr}, whereas a

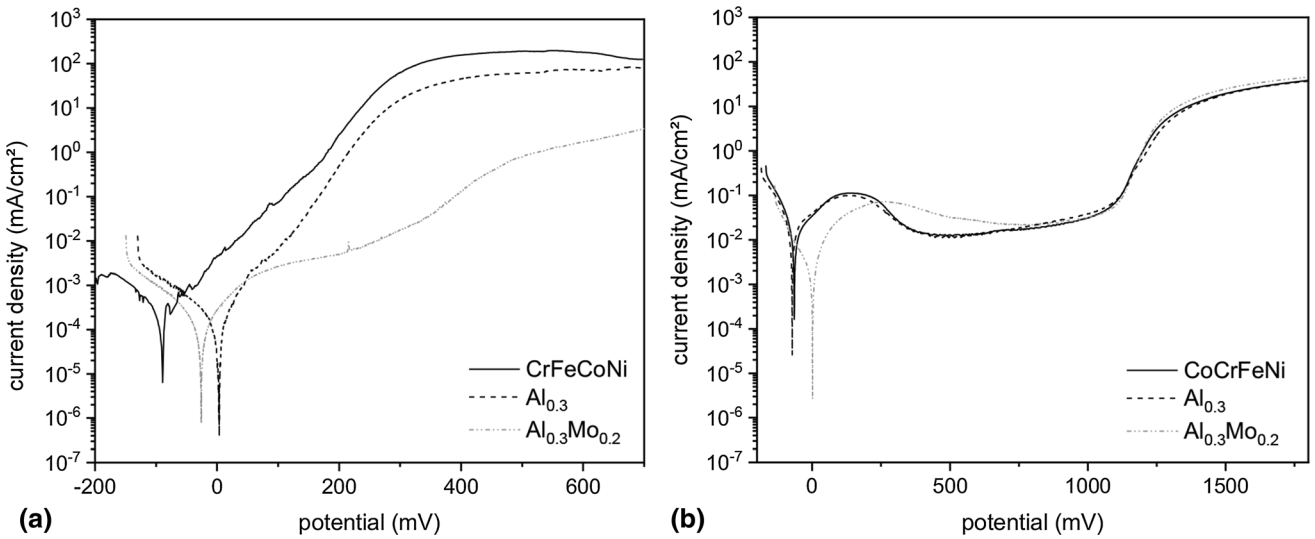

Fig. 6 Exemplary potentiodynamic polarization curves of CrFeCoNi, $Al_{0.3}$ and $Al_{0.3}Mo_{0.2}$ HVOF coatings: (a) 0.5 M NaCl electrolyte and (b) 0.05 M H_2SO_4 electrolyte

Table 5 Corrosion potential and corrosion current density of CrFeCoNi, $Al_{0.3}$ and $Al_{0.3}Mo_{0.2}$ HVOF coatings.

Alloy	Electrolyte	E_{corr}, mV	i_{corr}, mA/cm^2
CrFeCoNi	NaCl	…	…
CrFeCoNi	H_2SO_4	− 67 ± 2	(1.3 ± 0.2) × 10^{-2}
$Al_{0.3}$	NaCl	− 4 ± 8	(1.9 ± 0.6) × 10^{-4}
$Al_{0.3}$	H_2SO_4	− 73 ± 1	(1.3 ± 0.1) × 10^{-2}
$Al_{0.3}Mo_{0.2}$	NaCl	− 19 ± 8	(1.4 ± 0.3) × 10^{-4}
$Al_{0.3}Mo_{0.2}$	H_2SO_4	1 ± 2	(2.0 ± 0.2) × 10^{-3}

significant reduction is observed for the molybdenum-containing coating $Al_{0.3}Mo_{0.2}$. Therefore, it can be concluded that the element molybdenum dissolved in the solid solution significantly enhances the corrosion resistance of $Al_{0.3}Mo_{0.2}$ due to its passivating behavior.

For the investigation of the corrosion behavior, potentiodynamic polarization measurements have been conducted and interrupted at a defined current density (2 mA/cm2) in the vicinity of E_{corr}. The surface of the coatings has been investigated in the SEM subsequently. Exemplary images of the coatings tested in NaCl electrolyte are shown in Fig. 7.

For the corrosion measurements interrupted at a relatively low current density, localized pitting occurs for the CrFeCoNi and $Al_{0.3}$ coatings. However, the largest part of the coating surface shows no signs of corrosion attack. Such circular-shaped pits were also observed in $Al_{0.1}$-CrFeCoNi using a NaCl electrolyte (Ref 14). In contrast, no localized corrosion could be observed for the $Al_{0.3}Mo_{0.2}$ coating. Only minor structural defects, especially oxides and boundaries of the single spray particles, occur, which are also visible in the cross-sections of the coatings (Fig. 3). The absence of pitting corrosion in $Al_{0.3}Mo_{0.2}$ can be attributed to the passivating character of the element molybdenum (Ref 26). In addition, Gao et al. (Ref 10) as well as Tsau et al. (Ref 26) observed that molybdenum inhibits pitting corrosion in Cl^- containing solutions.

The investigation of the coatings in H_2SO_4 electrolyte revealed no distinct signs of corrosion after the tests interrupted at a current density of 2 mA/cm^2. Also, after full polarization only a thin surface layer with a thickness of approximately 10 µm is affected.

Summary and Conclusions

The influence of the alloying elements aluminum and molybdenum on the corrosion behavior of HEA CrFeCoNi HVOF coatings was investigated in detail. From the obtained results, the following findings can be drawn:

- The single-phase fcc structure of the inert gas atomized powder of the HEAs CrFeCoNi, $Al_{0.3}$CrFeCoNi and $Al_{0.3}$CrFeCoNi$Mo_{0.2}$ is retained due to the low thermal input during HVOF thermal spraying.
- The addition of aluminum and molybdenum to CrFeCoNi leads to an increase in hardness due to the increased atomic size of the alloying elements and the resulting pronounced lattice distortion. Moreover, the homogeneous microstructures produced by HVOF with its low content of structural defects further enhance the hardness.
- Potentiodynamic polarization measurements in NaCl and H_2SO_4 electrolytes reveal no significant influence

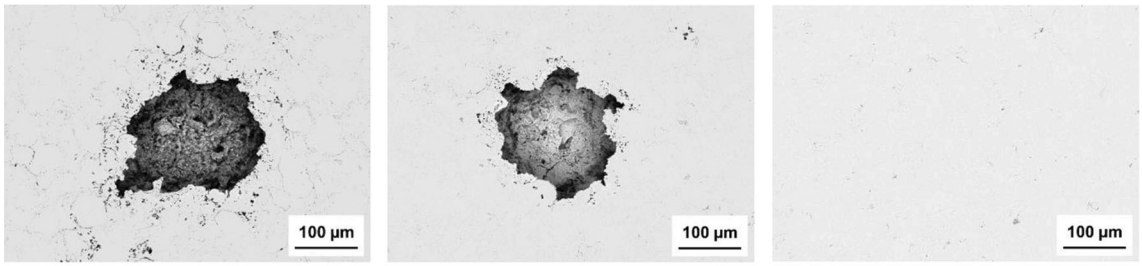

Fig. 7 Surface of HVOF coatings after potentiodynamic polarization measurements in NaCl electrolyte, interrupted at a current density of 2 mA/cm^2: (a) CrFeCoNi, (b) $Al_{0.3}$ and (c) $Al_{0.3}Mo_{0.2}$ coatings investigated in SEM (BSD)

on the corrosion behavior by adding aluminum to HVOF-coated CrFeCoNi. However, the element molybdenum causes a strong reduction of the corrosion current density, delayed pitting corrosion and hence an improved corrosion resistance if molybdenum is dissolved in the solid solution.

A further improvement of the functional coating properties can possibly be achieved by the application of alternative thermal spray processes, e. g. high-velocity air fuel thermal spraying (HVAF) or cold gas spraying (CGS), which enable a further reduction of structural defects especially pores and oxides. Due to the formation of a single-phase fcc structure, all investigated coatings exhibit a relatively low hardness. An approach for an increase is the incorporation of reinforcement particles or precipitates, which has to be investigated in subsequent studies.

Acknowledgments The authors gratefully acknowledge the financial support by the Sächsische Aufbaubank-Förderbank/SAB-100382175 by the European Social Fund ESF and the Free State of Saxony as well as the German Research Foundation (Deutsche Forschungsgemeinschaft/DFG), Project Number La-1274/54-1.

Funding Open Access funding enabled and organized by Projekt DEAL.

References

1. E.P. George, D. Raabe, and R.O. Ritchie, High-Entropy Alloys, *Nat. Rev. Mat.*, 2019, **4**, p 515-534. https://doi.org/10.1038/s41578-019-0121-4
2. M.-H. Tsai, A.-C. Fan, and H.-A. Wang, Effect of Atomic Size Difference on the Type of Major Intermetallic Phase in Arc-Melted CoCrFeNiX High-Entropy Alloys, *J. Alloys Comp.*, 2017, **695**, p 1479-1487. https://doi.org/10.1016/j.jallcom.2016.10.286
3. W. Zhang, P.K. Liaw, and Y. Zhang, Science and Technology in High-Entropy Alloys, *Sci. China Mater.*, 2018, **61**, p 2-22. https://doi.org/10.1007/s40843-017-9195-8
4. C. Li, J.C. Li, M. Zhao, and Q. Jiang, Effect of Aluminum Contents on Microstructure and Properties of AlxCoCrFeNi Alloys, *J. Alloys Comp.*, 2010, **504**, p 515-518. https://doi.org/10.1016/j.jallcom.2010.03.111
5. J. Joseph, N. Haghdadi, K. Shamlaye, P. Hodgson, M. Barnett, and D. Fabijanic, The Sliding Wear Behaviour of CoCrFeMnNi and Al_xCoCrFeNi High Entropy Alloys at Elevated Temperatures, *Wear*, 2019, **428-429**, p 32-44. https://doi.org/10.1016/j.wear.2019.03.002
6. J.-T. Liang, K.-C. Cheng, and S.-H. Chen, Effect of Heat Treatment on the Phase Evolution and Mechanical Properties of Atomized AlCoCrFeNi High-Entropy Alloy Powders, *J. Alloys Comp.*, 2019, **803**, p 484-490. https://doi.org/10.1016/j.jallcom.2019.06.301
7. M. Löbel, T. Lindner, S. Clauß, R. Pippig, and T. Lampke, Microstructure and Wear Behavior of the High-Velocity-Oxygen-Fuel Sprayed and Spark Plasma Sintered High-Entropy Alloy AlCrFeCoNi, *Adv. Eng. Mater.*, 2021 https://doi.org/10.1002/adem.202001253
8. T.-T. Shun, C.-H. Hung, and C.-F. Lee, The Effects of Secondary Elemental Mo or Ti Addition in $Al_{0.3}$CoCrFeNi High-Entropy Alloy on Age Hardening at 700 °C, *J. Alloys Comp.*, 2010, **495**, p 55-58. https://doi.org/10.1016/j.jallcom.2010.02.032
9. Y.X. Zhuang, X.L. Zhang, and X.Y. Gu, Effect of Molybdenum on Phases, Microstructure and Mechanical Properties of $Al_{0.5}$-CoCrFeMoxNi High Entropy Alloys, *J. Alloys Comp.*, 2018, **743**, p 514-522. https://doi.org/10.1016/j.jallcom.2018.02.003
10. M.C. Gao, J.-W. Yeh, P.K. Liaw, and Y. Zhang, *High-Entropy Alloys: Fundamentals and Applications*, Springer, Cham, 2016. https://doi.org/10.1007/978-3-319-27013-5
11. A. Sharma, High Entropy Alloy Coatings and Technology, *Coatings*, 2021, **11**(4), p 372. https://doi.org/10.3390/coatings11040372
12. Y. Qiu, S. Thomas, M.A. Gibson, H.L. Fraser, and N. Birbilis, Corrosion of High Entropy Alloys, *npj Mater. Degrad.*, 2017 https://doi.org/10.1038/s41529-017-0009-y
13. K. Yamanaka, H. Shriratori, M. Mori, K. Omura, T. Fujieda, K. Kuwabara, and A. Chiba, Corrosion Mechanism of an Equimolar

AlCoCrFeNi High-Entropy Alloy Additively Manufactured by Electron Beam Melting, *npj Mater. Degrad.*, 2020 https://doi.org/10.1038/s41529-020-00127-4
14. N. Kumar, M. Fusco, M. Komarasamy, R.S. Mishra, M. Bourham, and K.L. Murty, Understanding Effect of 3.5 wt.% NaCl on the Corrosion of Al01CoCrFeNi High-Entropy Alloy, *J. Nucl. Mater.*, 2017, **495**, p 154-163. https://doi.org/10.1016/j.jnucmat.2017.08.015
15. Y. Shi, B. Yang, and P.K. Liaw, Corrosion-Resistant High-Entropy Alloys: A Review, *Metals*, 2017, **7**(2), p 43. https://doi.org/10.3390/met7020043
16. Y.L. Chou, J.W. Yeh, and H.C. Shih, The Effect of Molybdenum on the Corrosion Behaviour of the High-Entropy Alloys $Co_{1.5}CrFeNi_{1.5}Ti_{0.5}Mo_x$ in aqueous environments, *Corros. Sci.*, 2010, **52**, p 2571-2581. https://doi.org/10.1016/j.corsci.2010.04.004
17. W. Wang, J. Wang, H. Yi, W. Qi, and Q. Peng, Effect of Molybdenum Additives on Corrosion Behavior of $(CoCrFeNi)_{100-x}Mo_x$ High-Entropy Alloys, *Entropy*, 2018, **20**, p 908. https://doi.org/10.3390/e20120908
18. X.-L. Shang, Z.-J. Wang, Q.-F. Wu, J.-C. Wang, J.-J. Li, and J.-K. Yu, Effect of Mo Addition on Corrosion Behavior of High-Entropy Alloys $CoCrFeNiMo_x$ in Aqueous Environments, *Acta Metall. Sin.*, 2019, **32**, p 41-51. https://doi.org/10.1007/s40195-018-0812-7
19. C. Dai, T. Zhao, C. Du, Z. Liu, and D. Zhang, Effect of Molybdenum Content on the Microstructure and Corrosion Behavior of $FeCoCrNiMo_x$ High-Entropy Alloys, *J. Mater. Sci. Technol.*, 2020, **46**, p 64-73. https://doi.org/10.1016/j.jmst.2019.10.020
20. J. Li, Y. Huang, X. Meng, and Y. Xie, A Review on High Entropy Alloys Coatings: Fabrication Processes and Property Assessment, *Adv. Eng. Mater.*, 2019, **21**(8), p 1900343. https://doi.org/10.1002/adem.201900343
21. A. Meghwal, A. Anupam, B.S. Murty, C.C. Berndt, R.S. Kottada, and A.S.M. Ang, Thermal Spray High-Entropy Alloy Coatings: A Review, *J. Therm. Spray Techn.*, 2020, **29**, p 857-893. https://doi.org/10.1007/s11666-020-01047-0
22. M. Oksa, E. Turunen, T. Suhonen, T. Varis, and S.-P. Hannula, Optimization and Characterization of High Velocity Oxy-fuel Sprayed Coatings: Techniques, Materials, and Applications, *Coatings*, 2011, **1**(1), p 17-52. https://doi.org/10.3390/coatings1010017
23. W. Scheider, Theory of the Frequency Dispersion of Electrode Polarization. Topology of Networks with Fractional Power Frequency Dependence, *J. Phys. Chem.*, 1975, **79**, p 127-136. https://doi.org/10.1021/j100569a008
24. Y.I. Kharkats, A.V. Sokirko, and F.H. Bark, Properties of Polarization Curves for Electrochemical Cells Described by Butler-Volmer Kinetics and Arbitrary Values of the Transfer Coefficient, *Electrochim. Acta*, 1995, **40**(2), p 247-252. https://doi.org/10.1016/0013-4686(94)00223-N
25. F. Fanicchia, I. Csaki, L.E. Geambazu, H. Begg, and S. Paul, Effect of Microstructural Modifications on the Corrosion Resistance of $CoCrFeMo_{0.85}Ni$ Compositionally Complex Alloy Coatings, *Coatings*, 2019, **9**(11), p 695. https://doi.org/10.3390/coatings9110695
26. C.-H. Tsau and M.-C. Tsai, The Effects of Mo and Nb on the Microstructures and Properties of CrFeCoNi(Nb, Mo) Alloys, *Entropy*, 2018, **20**(9), p 648. https://doi.org/10.3390/e20090648
27. Z. Niu, Y. Wang, C. Geng, J. Xu, and Y. Wang, Microstructural Evolution, Mechanical and Corrosion Behaviors of as-Annealed $CoCrFeNiMo\chi$ (χ= 0, 0.2, 0.5, 0.8, 1) High Entropy Alloys, *J. Alloys Compd.*, 2020, **820**, p 153273. https://doi.org/10.1016/j.jallcom.2019.153273